UDC539.24:669.15-177+669.71

Application of Field Emission Analytical Electron Microscopy to Metal Materials

Naoki Maruyama*1 Ryuji Uemori*1
Hirofumi Morikawa*2

Abstract:

In recent years, the performance of transmission electron microscopes has been improved. In particular, the emergence of field emission permits observation of the analytical electron microscopy (FE-AEM) arrangement of individual atoms, and the identification of the chemical composition of a microregion of the order of 1nm. This report summarizes the characteristics of FE-AEM. As an application to metal materials, the report briefly describes the results of FE-AEM analysis of a segregation of alloying elements in newly developed pearlitic steel wire with a strength of 2000 MPa, and the structure of ultrafine precipitates in Al-Mg-Si alloys.

1. Introduction

Since transmission electron microscopy (TEM) was first utilizesd in metallography, a great amount of knowledge has been obtained on the microstructures that govern the strength, ductility, toughness and other properties of materials. In particular, analytical transmission electron microscopy (AEM), which is a combination of TEM, energy dispersive X-ray spectroscopy (EDS) and electron energy loss spectroscopy (EELS), has made it possible to know not only the microstructure, but also the composition and the chemical state of a microregion. However, it was practically impossible for conventional AEM to determine the crystal structure and chemical composition of ultrafine precipitates of the order of nanometre, and also imposible to measure the seregation at the grain boundary or interphase interface.

The FE-AEM is an analytical transmission electron microscope equipped with a field emission gun (FEG). It provides information on the crystal structure, composition and chemical state of an ultra-microregion of a few nanometers ($1nm=10^{-9}m$). As ultrafine precipitates and the seregation of alloying elements affect mechanical properties directly or indirectly through various metallugical phenomena such as recrystallization and phase transformation, the control of microstructures in a nanometer region is an important goal of materials research. Therefore, the characterization tequniques, including FE-AEM, of an ultra-microregion are definitely playing a growing role.

Fig.1 shows typical microregion characterization techniques, compared in terms of spatial and depth resolution. Atom probe-field ion microscopy (AP-FIM) is worthy of mention as a characterization technique for image observation and compositional analysis of ultra-microregions of the atomic order. The AP-FIM technique is discussed in detail in another article in this issue. AP-FIM is disadvantageous in that it cannot analyze micrometer-order structures important in identifing the properties of materials. FE-AEM, however, can observe the overall state of microstructures from microscopic to a nanoscopic scale.

This article describes the performance and working principle of an FE-AEM equipped with EDS and EELS. The segregation behavior of alloying elements in pearlitic steel wire for a bridge cable with a strength of 2,000-MPa and the formation of ultrafine precipitates in a 6000 series aluminum alloy (Al-Mg-Si alloy) are briefly discussed as examples of the application of the FE-

*1 Technical Development Bureau

*2 Nippon Steel Techno Research Corporation

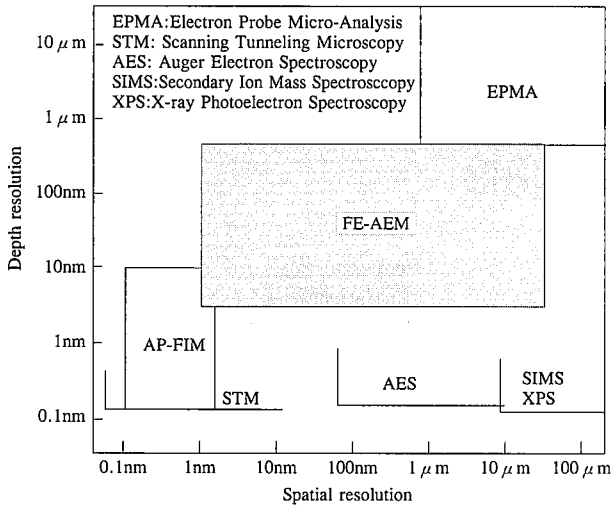

Fig. 1 Positioning of various microregion characterization techniques

AEM technique to metal materials.

2. Characteristics of FE-AEM

In FE-AEM, a field emission gun (FEG) is used as a electron sources in place of the conventional thermal emission gun (TEG), represented by tungsten (W) hairpin filament or a lanthanum hexaboride (LaB_6) filament. The FEG is effective in reducing the size of analytical regions and in improving the resolution of TEM images, in contrast to the TEG which uses thermal electrons as a source, because FEG uses the electrons produced by the field emission phenomenon at the tip of the filament, thus producing bright and coherent electron beam. The minimum diameter of the region that can be analyzed is about 30 nm for the conventional thermal emission TEM and about 1 nm for the FE-AEM. Electron holography is one interesting technique that takes advantage of the high coherency of the FEG[1].

Let us look at an example of the analytical capability of a FE-AEM (Hitachi HF-2000) used at Nippon Steel. **Fig. 2** shows the lattice image, nanoprobe EDS spectra, and EELS spectrum of a ultra-fine platelike precipitate in a vanadium bearing steel. A vanadium peak (see **Fig. 2**(b)) and carbon and nitrogen peaks (see **Fig. 2**(c)) are detected on the precipitate[2]. This means that the precipitate is a vanadium carbonitride. In the EDS spectra, vanadium is detected only at the central analytical point ②. This indicates that the spatial resolution of the analysis is 1 nm or less.

The FE-AEM can determine the amount of grain-boundary segregation in addition to the above-mentioned ultra-fine precipitates. **Fig. 3** shows the EDS concentration profiles of austenite grain boundaries in 17 mass% Cr-12 mass% Ni austenitic stainless steel sensitized at 600°C[3]. The chromium-depleted zone that had been difficult to measure by a conventional AEM is now clearly observable using an FE-AEM.

The principles of EDS and EELS, typical analytical techniques associated with the AEM, are briefly explained below.

EDS is based on the spectrometry of the characteristic X-rays emitted by the element of a specimen exposed to an incident electron beam focused on the specimen. EDS is the most popular TEM analytical technique because much applicable quantitative analysis software has been developed. The relation between the concentration ratio C_A/C_B for elements A and B, and measured

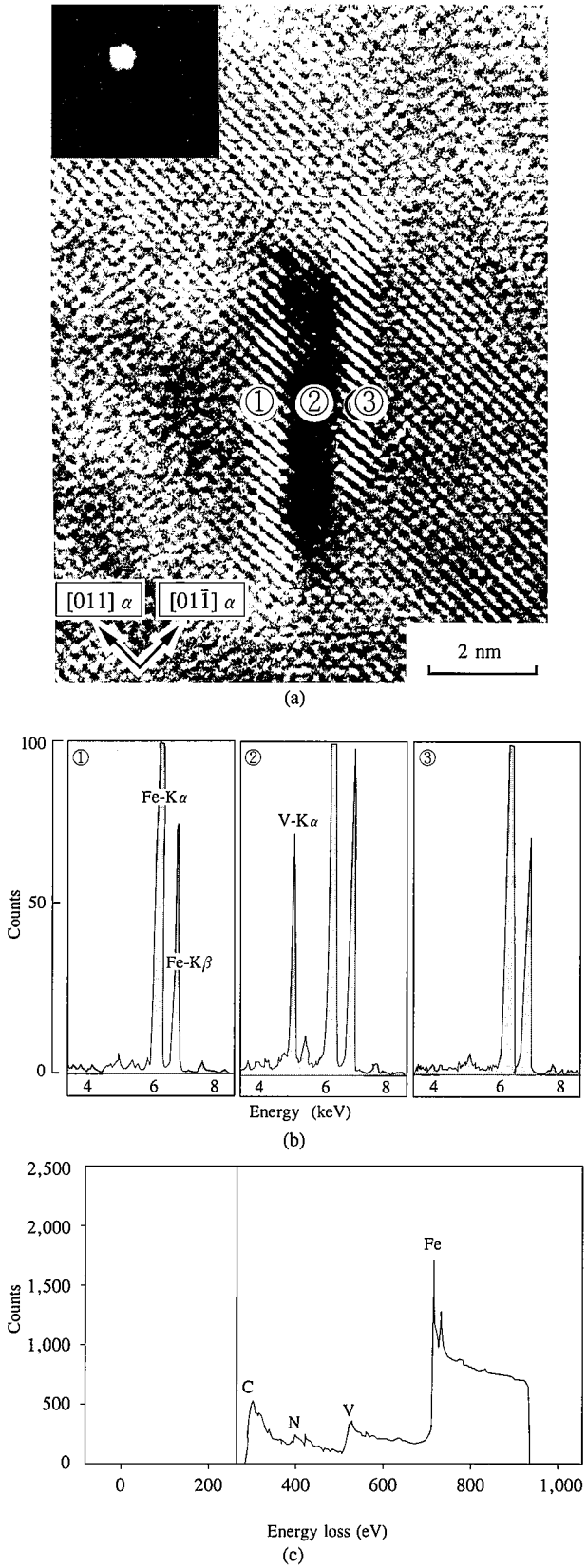

Fig. 2 High-resolution TEM image (a), EDS spectra (b), and EELS spectrum for ultrafine platelike precipitate in vanadium bearing steel. The bright spot at upper left in (a) shows the size of the analytical probe

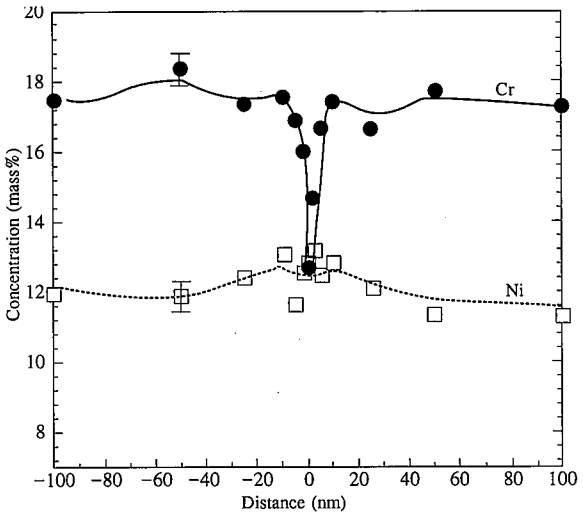

Fig. 3 EDS concentration profiles across an austenite grain boundary in austenitic stainless steel after sensitization

characteristic X-ray intensity ratio N_A/N_B for elements A and B is expressed by the following equation[4,5]:

$$\frac{C_A}{C_B}=k_{AB}\cdot\frac{N_A}{N_B}$$

where k_{AB} is the k-factor whose value depends on the sample and the instrument, including fluorescence yield, ionization cross-section, and detector efficiency. As evident from the above equation, the analytical accuracy of EDS depends on how accurately the k-factor is obtained. The k-factor can be determined theoretically (standardless method) or experimentally (standard method). The latter method can determine the concentration of the specimen more precisely, and is accurate to within a few percent. The analytical accuracy of the standardless method, which depends on such factors as the specimen and the film thickness, is within ±10%. The EDS quantitative analysis of light elements, such as boron, carbon, nitrogen and oxygen, calls for various corrections such as the absorption correction, involves a complicated procedure, and is rarely performed.

When electrons travel through the specimen, they lose energy due to their interaction with the atoms of the specimen. The interaction cross-section is related to chemical composition and atomic structure of the specimen. EELS technique is based on such energy loss of the electron. When attention is focused on a given inner-shell absorption edge (like K shell), the smaller the atomic number, the greater the scattering cross-section, with the result that detection sensitivity increases for lighter elements. For this reason, EELS is often used for the analysis of light elements, which is difficult by EDS. EELS can produce quantitative analysis with higher accuracy by using a standard sample of known concentration, which is also the case with EDS. However, since the spectral intensity and peak geometry of EELS depends to a great extent on such factors as the sample thickness, the chemical state of the specimen, the spectrum collection angle, and the TEM optical path, EELS compositional analysis is not as easy as EDS compositional analysis, and is not a general-purpose technique. For the working principle, quantitative analysis and other details of TEM/EELS, see references[6-8] at the end of this report.

3. Examples of the application of FE-AEM to the Study of Metal Materials

3.1 Effect of alloying elements on age softening of pearlitic steel wire with a tensile strength of 2,000 MPa

High-strength wire used in bridge cable is made by drawing out a eutectoid steel with a fine pearlite structure into wire, and hot-dip galvanizing the wire to impart corrosion resistance. The strength of steel wire can be increased, in principle, by increasing the amount of cold working, but the strength is limited in reality by a trade-off between ductility and strength (strength decreases when ductility increases) and the loss of strength (age softening) during the hot-dip galvanization. This section briefly describes the results of microstructural observation using the FE-AEM, focusing on the inhibiting effect of alloying elements on age softening, which is a key point in the development of 2,000-MPa tensile strength steel wire[9].

Table 1 shows the chemical compositions and heat treatment conditions of the steels used in the study. Steel A is a low-silicon manganese steel, steel B is a high-silicon manganese steel, while steel C is steel B with some of the manganese replaced by chromium. These steels correspond respectively to the chemical compositions of 1,600-MPa, 1,800-MPa, and 2,000-MPa steel wire. In **Fig. 4**, the loss of tensile strength (ΔTS) after aging at 450°C for 60 s, a simulating condition of hot-dip galvanization, is plotted against tensile strength before aging. **Photo 1** shows the TEM images of these steels after aging. Increasing the silicon content and adding chromium reduced the loss of tensile strength during aging. As cleanly shown in **Photo 1**, this is mainly due to

Table 1 Chemical compositions of steels

(mass%)

Steel	C	Si	Mn	Cr	Al
A	0.82	0.3	0.8	---	0.03
B	0.82	1.0	0.8	---	0.03
C	0.88	1.0	0.5	0.3	0.03
Experimental conditions	Austenitization(950°C)→Patenting(560-580°C) →Wire drawing→Aging(450°C×60s)				

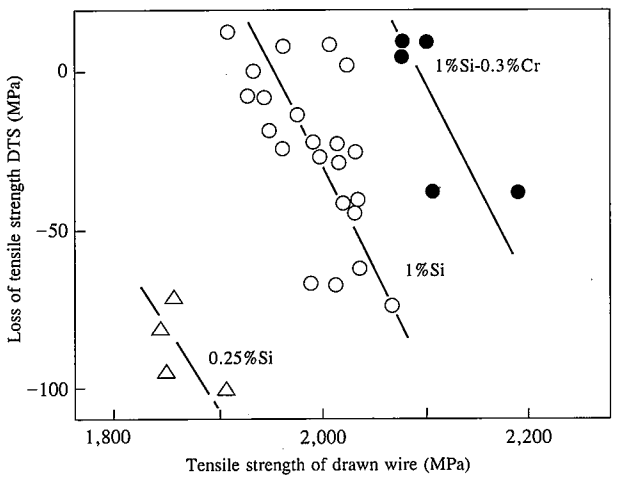

Fig. 4 Loss of tensile strength after aging at 450°C for 60 s in relation to tensile strength before aging

the retardation of the spheroidization (break-up) of cementite (the dark layers in **Photo 1**).

Fig. 5 is a high-resolution image and shows the concentration profiles of silicon, manganese and chromium across the cementite θ /ferrite (α) interface after aging steel C at 450°C. The diameter of the probe is 1 nm, and the distance between the points is a minimum of 2 nm. The compositional analysis used the EDS standardless method. The concentration profiles clearly reveal the segregation of silicon in the ferrite near the interface, and the concentration of chromium and manganese in the cementite. As the diffusion coefficient of silicon in ferrite is lower than the self-diffusion coefficient[12], it may be concluded that the rate of the spheroidization of the lamellar cementite is controlled by the diffusion of the silicon segregated at the θ / α interface. This is also supported by the fact that the spheroidization rate equation for lamellar pearlite is confirmed by the cubic law[10].

The chromium and manganese also retard the spheroidization of the cementite. A report[11] concerning the effects of chromium and manganese on the growth of cementite particles suggests that the growth of cementite particles is controlled by the diffusion of substitutional elements, such as chromium and manganese, in ferrite. The impurity diffusion coefficients of chromium and manganese in ferrite at 450°C are 6.2×10^{-22} and 1.9×10^{-21} m^2/s[12], respectively, and the diffusion of chromium in ferrite is slightly slower than for manganese. In our results, the partition coefficient (C_θ/C_α) of the cementite/ferrite was 3.7 for chromium and 2.5 for manganese, and the coefficient of chromium is higher than manganese. Therefore, it may be concluded that the reason why the steel C with chromium shows greater retardation of the spheroidization of cementite than steel B is that chromium has a lesser tendency to diffuse than manganese and a greater tendency to concentrate in cementite.

3.2 Precipitation behavior in 6000-series aluminum alloy

6000-series aluminum alloys (Al-Mg-Si alloys) have excellent strength, formability and corrosion resistance, and are expected to be used as a weight-saving material for body panels and other automotive components. The 6000-series aluminum alloys are characteristic in that desired strength properties can be obtained by making use of precipitates in aging. Control of precipitation is thus extremely important in obtaining good strength properties.

The precipitation sequence in the Al-Mg-Si alloys is also metallurgically interesting and has been investigated by many researchers[13-16]. The precipitation occurs through a complicated process consisting of clusters, needlelike Guinier-Preston (GP) zones, β '-Mg_2Si intermediate phases, and β -Mg_2Si equilibrium phases[13]. These precipitate phases are so fine that their precipita-

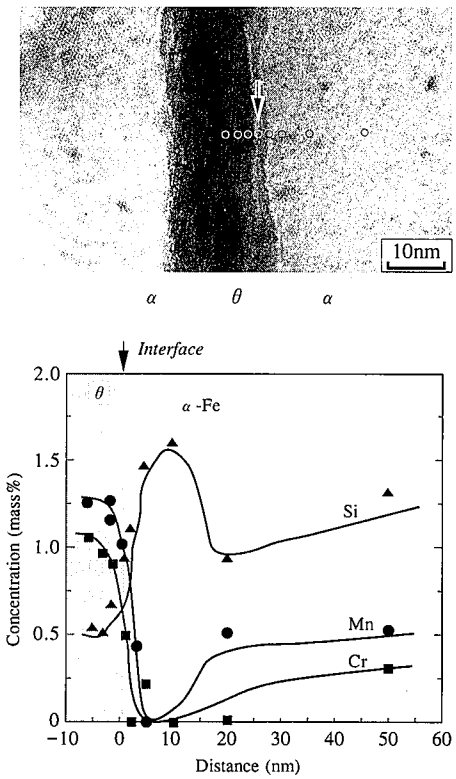

Fig. 5 High-resolution transmission electron micrograph and the concentration profiles of silicon, manganese and chromium across the cementite(θ)/ferrite(α) interface in steel C after aging at 450°C

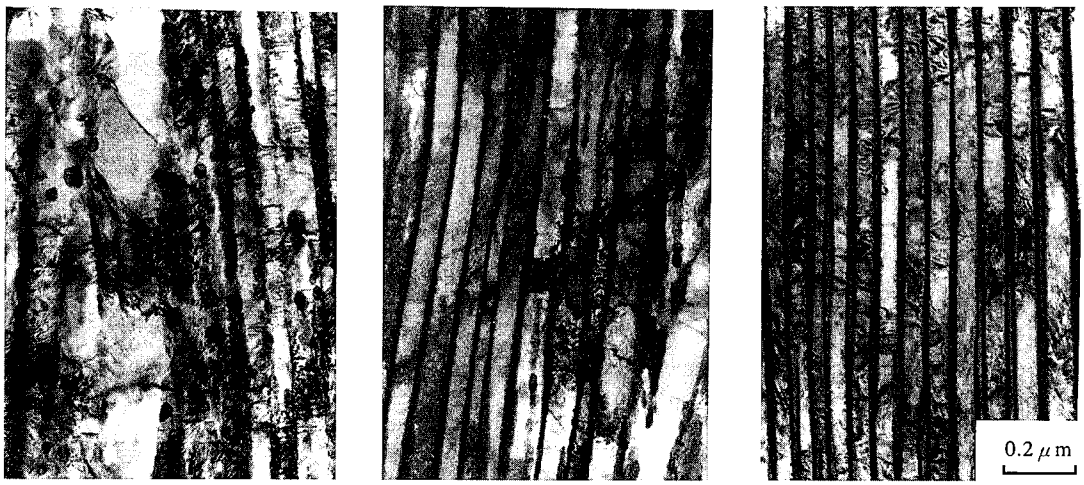

(a) Low Si-Mn steel (steel A) (b) High Si-Mn steel (steel B) (c) High Si-Mn-Cr steel (steel C)

Photo 1 TEM microstructures of steel A, B and C after aging

tion behaviors, including their composition and structure, still remain unclear. In this section, the structural and compositional analysis of ultrafine precipitates in Al-Mg-Si alloys are described as an example of the FE-AEM analysis[17,18].

An Al-0.064 mass% Mg-0.81 mass% Si alloy was solution treated at 550°C for 30 minutes, rapidly cooled in ice water, and aged at 175°C for nine hours and at 250°C for one hour to obtain various phases of precipitates. TEM specimens were cooled to -20°C, thinned by electropolishing at -20°C in a 2:1 solution of nitric acid and methanol, and subsequently cleaned with Ar^+ ions to remove the oxide layer. The composition of the precipitates was quantitatively analyzed using the EDS standardless method, while their structure was analyzed by the electron diffraction method.

Photo 2 shows the TEM images of specimens aged at 175°C for nine hours and at 250°C for one hour, respectively. The specimens aged at 175°C corresponds to the initial stage of the aging treatment and reveals finely dispersed precipitate phases. The precipitates are needle-like and elongated in the <100> direction of the aluminum matrix. The length of the elongated direction is 10-100nm and 100-500nm, while the cross-sectional diameter in the longitudial direction is about 2nm and 5-10nm.

Fig. 6 shows high-resolution images of precipitates observed from longitudinal direction, and the EDS spectra of the precipitate. Their magnesium/silicon composition ratio was 1.00±0.04 for the 175°C aged sample and 1.21±0.04 for the 250°C aged sample. FE-AEM was able to reveal the compositional changes of these ultrafine precipitates hither to in accessible to conventional AEM.

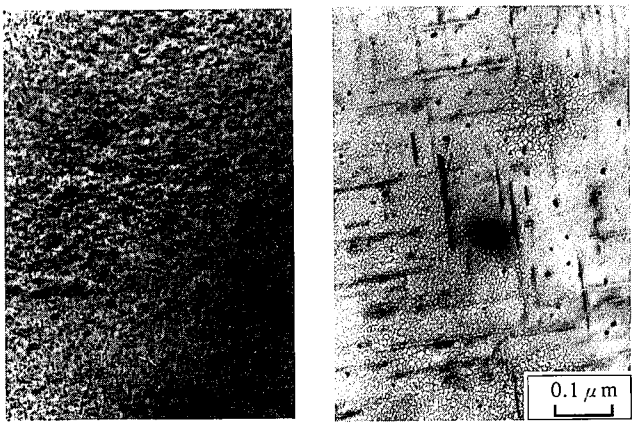

(a) Aged at 175°C for 9 h (b) Aged at 250°C for 1 h

Photo 2 TEM images of samples aged at 175°C and 250°C, respectively (electron beam was aligned to <001> direction of Al matrix)

The electron diffraction patterns of the precipitates present in the aged specimen are shown in **Photo 3**, and their structural analysis results are given in **Table 2**. The probe diameter is about 2 nm. The results of structural analysis show that three precipitate phases, β'' with a hexagonal structure, β' with a orthorhombic

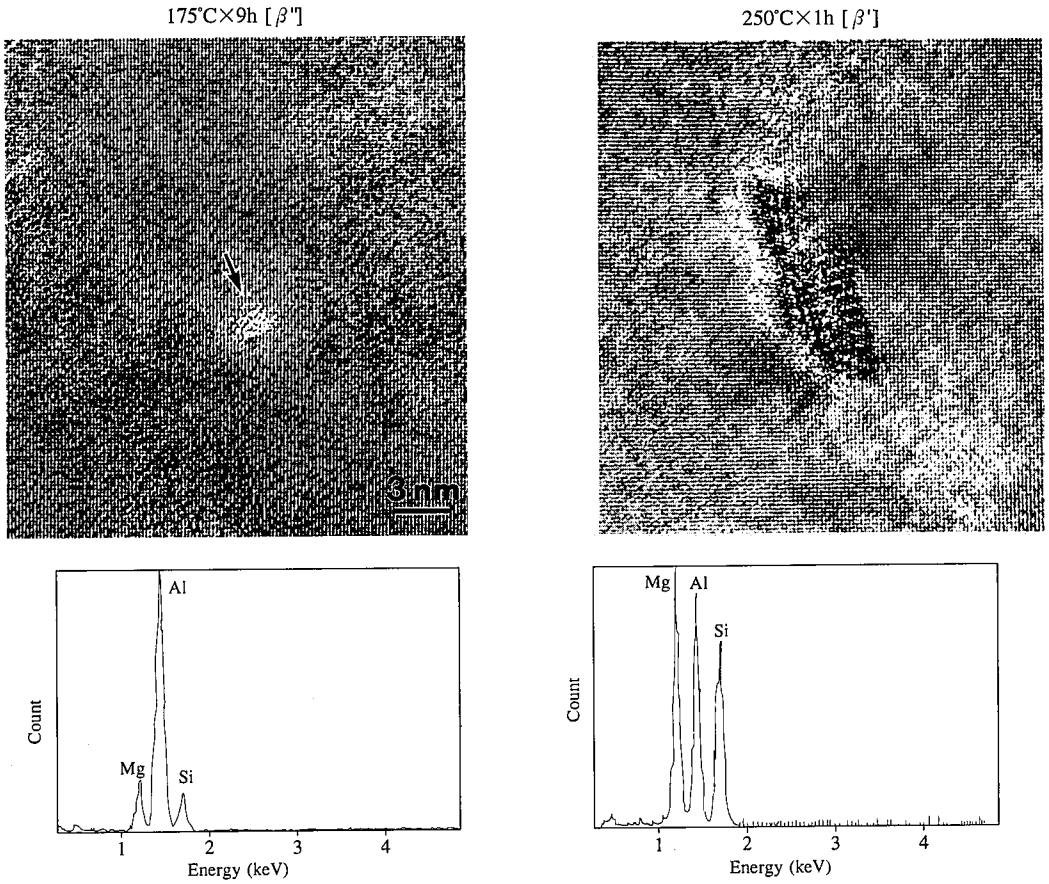

Fig. 6 High-resolution transmission electron micrographs and nanoprobe EDS spectra of ultrafine precipitates in specimens aged at 175°C and 250°C, respectively

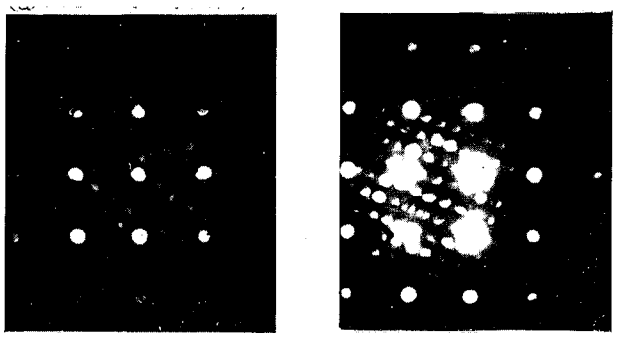

(a) Monoclinic β "(175°C×9h) (b) Orthorhombic β '(250°C×1h)

Photo 3 Electron diffraction patterns of precipitate in specimens aged at (a) 175°C and (b) 250°C, respectively (electron beam aligned to longitudinal direction of precipitates)

Table 2 Results of structural analysis of precipitates

	Structure of precipitates and orientation relationship between precipitates and Al matrix
175°C aging	*Monoclinic* β " a=0.714±0.017, b=0.658±0.013, c=0.405[mm], γ =75±1° ◇$[001]_{\beta''}$//$[001]_{Al}$ ◇$[100]_{\beta''}$//$[3\bar{1}0]_{Al}$ ($[010]_{\beta''}$//$[230]_{Al}$)
250°C aging	*Hexagonal* β ' a=0.705,c=0.405[mm] ◇$[001]_{\beta'}$ //$[001]_{Al}$ ◇a-type $[100]_{\beta'}$ //$[100]_{Al}$ b-type $[100]_{\beta'}$ ∠$[100]_{Al}$=18-22° c-type $[100]_{\beta'}$ //$[\bar{1}10]_{Al}$ · $[100]_{\beta'}$ //$[110]_{Al}$
	Orthorhombic β " a=0.672±0.003, b=0.787±0.003, c=(0.405)[nm] ◇$[001]_{\beta'}$ //$[3\bar{1}0]_{Al}$ · $[100]_{\beta'}$ //$[310]_{Al}$

structure, and β " with a monoclinic structure, β ' are present in the specimen aged at 250°C, and β " is present in the specimen aged at 175°C. The results clearly shows the existance of β " phase in precipitation sequence. Therefore, it is supposed that the initial precipitation of Al-Mg-Si alloys proceeds as follows: Coherent GP →semicohent β " (monoclinic) →semicohent β ' (hexagonal and orthorhombic). The β " precipitates are dispersed in large amounts in aluminum alloys that exhibit the highest hardness, and the precipitates play an important role in strengthening aluminum alloys.

5. Conclusion remarks

To control the microstructures that govern the properties of materials, it is vital to quantitatively grasp the relationships between microstructural features, such as precipitates, grain-boundary segregation and dislocations, and metallurgical phenomena, such as recrystallization, grain growth and phase transformation. This quantitative knowledge is essential not only for developing new functional materials in pursuit of ultimate performance, but also for designing more efficient material compositions and material manufacturing processes. Conventional material research has been based on these needs, but has been limited in the examination of actual phenomena because of the limitations of available analytical techniques. The information obtained by the FE-AEM introduced in this article has a great impact on materials research in terms of precipitation, segregation and other metallurgical phenomena. When used in combination with AP-FIM, which is an atomic order analytical technique, and X-ray diffraction and electron probe X-ray microanalysis (EPMA), which are macroscopic analytical techniques, FE-AEM will add impetus to the research and development of materials.

References

1) Tonomura, A.: J. Surf. Sci. Soc. of Japan. 13, 546 (1992)
2) Ikematsu, Y. et al.: Electron Microscopy. 2, 265 (1992)
3) Maruyama, N. et al.: 8th Tech. Forum of Electron Microsc. Jap. Soc. of Electron Microsc. 1995, p. 1
4) Cliff, G. et al.: J. Microscopy. 103, 230 (1975)
5) Shindo, D.: 10th Forum of Anal. Electron Microsc. Jap. Soc. of Electron Microsc. 1994, p. 1
6) Egerton, R.F.: Electron Energy Loss Spectroscopy in the Electron Microscope. Plenum Press, 1984
7) Kurata, H.: 10th Forum of Anal. Electron Microsc. Jap. Soc. of Electron Microsc. 1994, p. 4
8) Budd, P.M. et al.: Light-Element Analysis in the Transmission Electron Microscope. WEDX and EELS, Oxford Science Publications, 1988
9) Takahashi, T. et al.: CAMP-ISIJ. 7, 777 (1994)
10) Tarui, T. et al.: 35th MWSP Conf. Proc. ISS-AIME, Vol. XXXI, 1994, p. 231
11) Sakuma, T.: Bulletin of Jpn. Inst. Met. 20, 247 (1981)
12) Smithhells Metals Reference Book. 7th ed. Section 13-19, Butterworth Heinemann, 1992
13) Kanno, M. et al.: J. Jap. Inst. of Light Metals. 28, 553 (1978)
14) Jacobs, M. H : Phil. Mag. 26, 1 (1972)
15) Saga, M. et al.: 88th Conf. of Jap. Inst. of Light Metals. 1995, p. 111
16) Maruyama, N.et al. : Scripta Mat. (to be published)
17) Dutta. I, et al. : J.Mator. Sci. Lett. 10, 323 (1991)
18) Edwards, G. A. et al. : Appl. Surf. Sci. 76/77, 219 (1994)